PERGAMON

Corrosion Science 44 (2002) 841–860

CORROSION SCIENCE

www.elsevier.com/locate/corsci

Quantitative evaluation of general corrosion of Type 304 stainless steel in subcritical and supercritical aqueous solutions via electrochemical noise analysis

X.Y. Zhou [a,*], S.N. Lvov [b], X.J. Wei [c], L.G. Benning [d], D.D. Macdonald [e]

[a] *The Energy Institute, The Pennsylvania State University, 222 Academic Project Bl., University Park, PA 16802, USA*

[b] *Department of Energy and Geo-Environment Engineering, The Pennsylvania State University, 207 Research East Bl., University Park, PA 16802, USA*

[c] *The Energy Institute, The Pennsylvania State University, 209 Academic Project Bl., University Park, PA 16802, USA*

[d] *School of Earth Sciences, University of Leeds, Leeds LS2 9JT, UK*

[e] *Department of Materials Science and Engineering, The Pennsylvania State University, 0201 Sterdle Bl., University Park, PA 16802, USA*

Received 19 January 2001; accepted 10 April 2001

Abstract

Electrochemical noise (EN) sensors have been developed to measure the corrosion rate of Type 304 stainless steel (**SS**) in subcritical and supercritical environments. The EN sensors were tested in flowing aqueous solutions containing NaCl and HCl at temperatures from 150°C to 390°C, a pressure of 25 MPa, and flow rates from 0.375 to 1.00 ml/min. The potential and coupling current noise were recorded simultaneously and the noise resistance (R_n) was calculated from the standard deviations in the potential and current records. We found that the inverse noise resistance correlated very well with the corrosion rate evaluated from separate mass loss experiments, and that both the inverse noise resistance and the average corrosion rate were functions of temperature and flow rate. In the temperature range from 200°C to 390°C, the corrosion rate was found to be proportional to the inverse noise resistance and hence the Stern–Geary relationship can be used to evaluate the corrosion rate. However, at

* Corresponding author. Fax: +1-814-865-3573.
E-mail address: xxz15@psu.edu (X.Y. Zhou).

0010-938X/02/$ - see front matter
PII: S0010-938X(01)00088-9

150°C, the relation between inverse noise resistance and corrosion rate significantly deviated from the Stern–Geary relationship. It was found that the deviation was related to the low corrosion rate of Type 304 SS and 150°C.

Keywords: Electrochemical noise analysis; Supercritical solution; Noise resistance

1. Introduction

Spontaneous fluctuations of electrode potential and current in an electrochemical system are known as electrochemical noise (EN). Electrochemical noise analysis (ENA) is a unique technique among all electrochemical methods that have been used in corrosion research, because: (1) it can be conducted under open circuit conditions; (2) it needs no externally imposed perturbation of the system that could lead to changes in system-specific properties; (3) the spontaneous fluctuations in current and voltage are normally sufficiently small that the constraints of linear system theory are satisfied. The acquisition of EN data requires a comparatively simple experimental setup that can be conveniently used for in situ monitoring.

Ever since EN in corrosion processes was first reported in the sixties [1,2], the application of ENA has developed rapidly. Early studies focussed on exploring the correlation between corrosion rate and potential, current, and other characteristics of EN [3–5]. These approaches proved to be suitable for studying localized corrosion, such as pitting and stress corrosion cracking. However, potential or current monitoring can only provide a qualitative assessment of the corrosion processes. Later work was directed towards simultaneously monitoring the potential and coupling current from two coupled identical electrodes [6–13]. The results of these studies show that this method can be used to quantitatively evaluate corrosion rate. The most important step of the method is the determination of the noise resistance (R_n), which is defined as the ratio of the standard deviations of the potential noise (σ_E) and coupling current fluctuations (σ_I):

$$R_n = \frac{\sigma_E}{\sigma_I} \tag{1}$$

Eden et al. [6] and Chen and Skerry [7] suggested that R_n should be related to the polarization resistance (R_p) that was commonly determined by linear polarization techniques or electrochemical impedance spectroscopy (EIS). Initially, R_n was thought to be equivalent to R_p and hence the corrosion current density (i_{corr}) was evaluated using the Stern–Geary relationship [6,7]:

$$i_{corr} = B\left(\frac{1}{R_p}\right) \tag{2}$$

where B is a constant. It was found later that, in reality, R_n was not always equal to R_p but rather that R_n was related to R_p indirectly. Bertocci et al. [14] derived the relationship between R_n and the spectral resistance, R_{sn}:

$$R_n = \left[\frac{\int_{f_{min}}^{f_{max}} \Psi_I(f) R_{sn}^2(f)\, df}{\int_{f_{min}}^{f_{max}} \Psi_I(f)\, df} \right]^{1/2} \tag{3}$$

where $\Psi_I(f)$ is the power spectrum density (PSD) of the coupling current, f is the frequency in Hertz, f_{min} is the lower limit of the frequency (equal to two times the inverse measurement time), f_{max} is the higher limit frequency (equal to one-half of the sampling frequency). The spectral resistance itself is defined by

$$R_{sn} = \left[\frac{\Psi_V(f)}{\Psi_I(f)} \right]^{1/2} \tag{4}$$

where $\Psi_V(f)$ is the PSD of the potential. If f_{min} is sufficiently low (i.e., the acquisition time is sufficiently long), R_n can be expressed by

$$R_n = R_{sn}(f \to 0) \tag{5}$$

Through theoretical analysis with a minimum of assumptions, Bertocci et al. [14,15] found that for the case in which: (1) the EN sensor consisted of two identical, coupled electrodes and a noiseless reference electrode; (2) instrumentation noise was negligible in comparison to the "true" EN, and; (3) the solution resistance was negligible in comparison to the electrode impedance, the following equalities existed:

$$R_n = R_{sn}(f \to 0) = Z(f = 0) = R_p. \tag{6}$$

In Eq. (6), $Z(f = 0)$ is the electrochemical impedance at zero frequency. These relationships were verified experimentally [11,12] for the cases of bare electrodes and coated electrodes with defects. Note that there were other cases in which Eq. (6) cannot be applied [8–13], because the conditions for the relations were not completely satisfied.

Previously, only a few attempts have been made to explore the possibility of using ENA for monitoring corrosion at high temperatures. Thus, Liu et al. [16] and Macdonald et al. [17] measured the coupling current between two identical steel electrodes and, using a band-pass filter and a root-mean-square (rms) converter, defined the "corrosion activity" (CA) as the amplitude of the resulting signal over a pre-selected bandwidth in frequency. The CA was found to change sensibly with variations in important parameters, such as pressure and flow rate. In particular, the CAs for carbon steel and Type 304 stainless steel (SS) in oxygenated water and dilute HCl solutions, respectively, were found to pass through maxima at temperatures that are slightly below the critical temperature of water (376.15°C). These measurements were carried out at unprecedented temperatures of up to 498°C.

Manahan et al. [18] measured the noise in the coupling current between an insulated (PTFE coated), sensitized Type 304 (SS) fracture mechanics specimen containing an active corrosion crack and external (platinized Ni) cathodes in water at 250°C. The coupling current was found to contain periodic noise that occurred in packages of 4–13 fluctuations. These pulses were attributed to brittle microfracture events occurring at the crack tip. Later work [19] has shown similar fracture induced

pulses during caustic cracking in AISI 4340 steel at 70°C. Still other work has demonstrated that a linear relationship exists between crack growth rate and the mean coupling current for intergranular fracture in sensitized Type 304 SS in water at 250°C [20]. This linear relationship has been proposed to be a sensitive method for measuring very low crack growth rates, because of the ease with which small currents can be measured.

Due to their unusual properties, high subcritical and supercritical aqueous solutions have many important industrial applications. However, high subcritical and supercritical aqueous solutions are extremely corrosive environments for many metallic materials. Corrosion problems hinder the use of high subcritical and supercritical aqueous solutions in many applications. Thus, the development of an in situ technique for monitoring electrochemical and corrosion processes in high subcritical and supercritical environments will not only benefit technical areas, such as power generating, chemical, geothermal, oil refining, and supercritical water oxidation industries in terms of corrosion control, but will also offer an unique and powerful tool for elucidating the mechanisms of metallic corrosion under such extreme environments.

The present paper is concerned with the use of ENA to quantitatively evaluate the general corrosion rate of Type 304 SS in high subcritical and supercritical ($T >$ 374.15°C) aqueous systems. To date, it has not been demonstrated in any of the previous studies that the measured noise resistance correlates with general corrosion rate over this extended range in temperature, which includes the transition from the subcritical to the supercritical states.

2. Experimental approach

2.1. Electrochemical noise sensors

There were two major challenges in developing the electrochemical sensors suitable for use in high temperature, high pressure environments. The first one is the sealing problem. The sensing electrodes should be exposed to the high temperature solution in which these electrodes are supposed to work, but all other parts of the electrodes should not be in contact with the solution. Furthermore, the sealing system should be such so as to avoid crevice corrosion. Secondly, there exists the problem of contamination of the working solution, due to the dissolution of the metallic components of the experimental system under the high temperature aqueous conditions. In the worst case, the composition could change dramatically during data acquisition and an electrochemical steady state may never be achieved. We have employed a number of techniques to solve these problems in the study.

The EN sensor used here consisted of three electrodes. As shown in Fig. 1, two of the electrodes were Type 304 SS wires with a diameter of 0.50 mm made from the same roll of virgin material. The third electrode was a platinum wire with a diameter of 0.50 mm. The wires were inserted into a three-hole ceramic tube and initially both

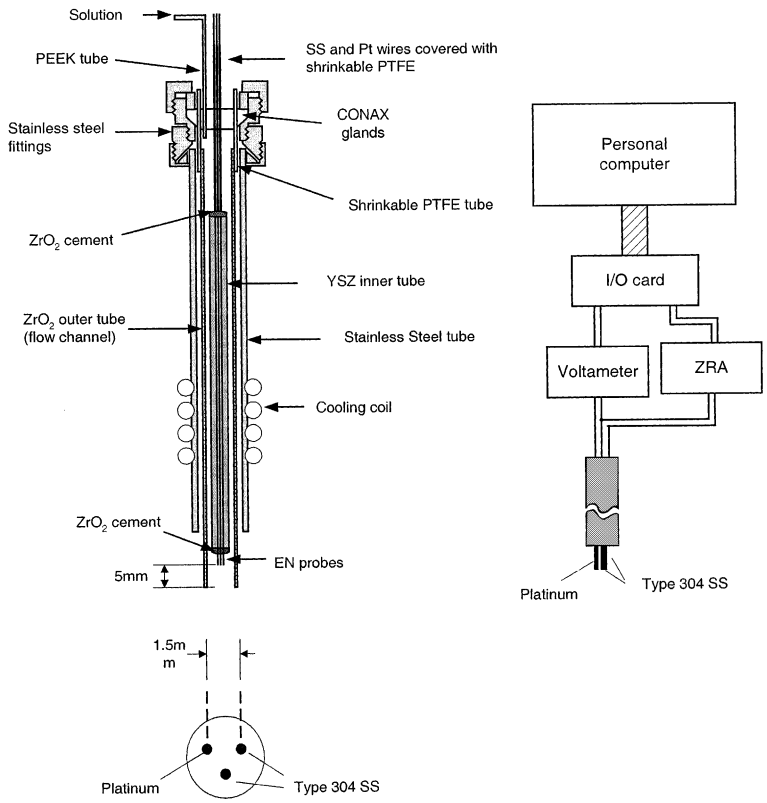

Fig. 1. Schematics of the EN sensor and data acquisition system.

ends of the wires were exposed. The distance between the holes was 1.5 mm. The extra space in the holes was filled with high temperature zirconia (ZrO_2) cement, which was also used as the sealant for the ends of the tube. When the cement had dried under ambient conditions, the entire assembly of the ceramic tube was heat-treated in vacuum at 800°C for 24 h.

After being heat-treated, each of the exposed wires was cut to assure that a length of 10 mm protruded from one end of the tube. These wires were slightly polished, washed with acetone and deionized water, and then dried. This part of the assembly was prepared for exposure to high temperature solutions.

The other exposed parts of the wires were first covered with shrinkable PTFE tubing. The ends of the PTFE tubes were pre-etched using an oxidizing solution. An epoxy cement was used to fill the small gaps between the PTFE tube and the ceramic tube. The PTFE-shielded wires were then installed in a standard CONAX gland. This part of the assembly was maintained at ambient temperature in our experiment. In addition to the wires, a PEEK capillary, which served as the solution inlet, was also installed in the CONAX glands.

Finally, the entire assembly was placed inside a flow channel made from a YSZ tube in the high temperature zone and a heat-shrinkable PTFE tube in the low temperature zone. Thus, the test solution coming from the PEEK capillary was not in contact with any metallic surface before reaching the electrodes. The ends of the electrodes were located at a distance of 10 mm from the end of the outer zirconia tube, so that any contamination from outside of the channel was impossible when flow existed in the channel.

The flow channel was placed in a stainless steel tube for maintaining the sensor in the high pressure/temperature solution. The stainless steel tube was connected to the CONAX gland at one end and to a hydrothermal cell on the other end.

During the course of the present experiments, a test solution was fed in from the PEEK inlet using a metal-free HPLC pump. Since the test solution contacted either plastic or ceramic surfaces, and because the solution was constantly renewed, contamination of the high temperature solution inside the flow channel was minimized.

2.2. High temperature electrochemical cell

A flow-through electrochemical cell (Fig. 2), similar to the one described in Refs. [21–24], was used in the present experiments. The body of the cell was made from a stainless steel union cross with four ports occupied with the following electrodes or sensors: (1) a flow-through external reference electrode [23]; (2) the EN sensor; (3) a

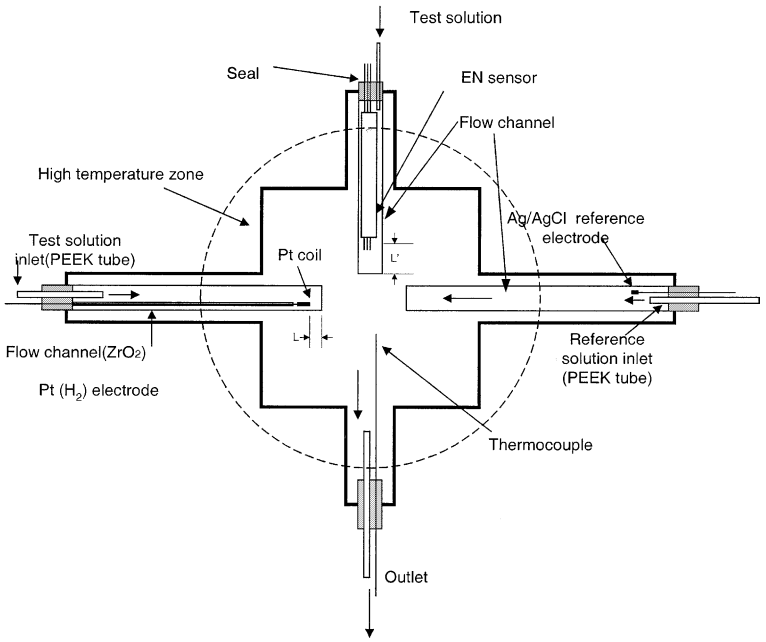

Fig. 2. Schematic of the hydrothermal electrochemical cell.

flow-through hydrogen (Pt) electrode [23]; and (4) a solution outlet and a thermocouple. The reference and Pt electrodes were placed in zirconia channels and were employed for monitoring the pH in the hydrogenated solution.

Heating of the electrochemical cell was effected by band heaters, and a pressure of 25 MPa was maintained using a pressure relief valve. The temperature and pressure were controlled to ±0.2°C and ±0.35 MPa, respectively.

2.3. Data acquisition system

The coupling current between the two identical stainless steel wires of the EN sensor was measured using a zero resistance ammeter (ZRA) (Fig. 1). The Pt wire of the EN sensor was employed as a reference electrode. The potential of the coupled stainless steel electrodes against the Pt electrode was measured using a programmable Keithley electrometer. The analog outputs of the electrometer and the ZRA were first transferred to an amplifier and then were converted into digital signals via a National Instrument A/D board operated by a LABVIEW program. As a compromise between accuracy, bandwidth, and acquisition rate of the data acquisition system, we chose a sampling frequency of 4 Hz and a sampling time of 512 s. In other words, each acquired data set consisted of 2048 readings.

To evaluate the noise level of the instrument, a dummy cell, comprising a resistor of 100 Ω or 10 kΩ, was connected to the data acquisition system. We found that the noise level of the potential was less than 0.1 mV and that of the current was less than 2 nA. In other words, the instrument noise levels were much lower than the noise levels we detected from the EN sensors.

2.4. Experimental procedure

The first task of the experimental procedure was to verify the reliability and accuracy of the pH monitoring system, which consisted of the flow-through reference and Pt electrodes. The procedure has been fully described in Refs. [23,24]. Briefly, two hydrogen-saturated solutions ($[H_2] = 7.84 \times 10^{-4}$ mol kg^{-1}), 0.1 mol kg^{-1} NaCl + 0.01 mol kg^{-1} HCl (Solution 1) and 0.1 mol kg^{-1} NaCl + 0.001 mol kg^{-1} HCl (Solution 2), were consecutively pumped into the flow-through Pt electrode. The solution that was pumped through the external reference electrode was always 0.1 mol kg^{-1} NaCl from a reservoir purged with helium gas. The potentials of the Pt electrode for both solutions were measured against the same external reference electrode. The difference in the potentials for the two solutions was compared to the calculated value, as described in Refs. [24,25]:

$$\frac{\Delta E - \Delta E_d}{(RT/F)\ln 10} = \log\left(\frac{m_{HCl}(S1)}{m_{HCl}(S2)}\right) = -\Delta pH \tag{7}$$

where ΔE is the calculated potential difference, ΔE_d is the residual diffusion potential, $m_{HCl}(S1)$ and $m_{HCl}(S2)$ are the analytical concentrations of HCl in solutions 1 and 2, respectively, and ΔpH is the pH difference of the two solutions at the experiment

temperature. As an example, we found that the potential difference measured at 150°C was 75 ± 2 mV, while the calculated value was 78 mV. Thus, the pH monitoring system is able to measure a pH difference with a precision of ± 0.05 units.

The second step in this study was to acquire EN signals from the EN sensor in 0.1 mol kg^{-1}, NaCl + 0.01 mol kg^{-1} HCl + H_2 mol kg^{-1}, while the pH was monitored using the Pt electrode and external reference electrode. The test solution was directed to the EN sensor and to the Pt electrode from a reservoir that was purged with high purity hydrogen gas. All solutions used in the experiment were prepared gravimetrically from Millipore deionized water and reagent grade chemicals using Pyrex glassware and a high precision balance (± 0.0001 g). We conducted five tests at 150°C, 200°C, 250°C, 300°C, 350°C, and 390°C. The variation in temperature was found to be ± 0.2°C. For each of these experiments, we used four different flow rates: 0.375, 0.5, 0.75 and 1.0 ml/min. The precision of flow rate control was 2% of the set flow rate. For all of the experiments, the pressure in the electrochemical cell was 25 ± 0.35 MPa. We made a number of identical EN sensors. Each of them was used in only one test.

2.5. Mass loss tests

The mass loss tests were conducted in the same electrochemical cell, but not coincidentally with the noise experiments. Instead of an EN sensor, a stainless steel coil cut from the same roll of stainless steel wire that was used to fabricate the noise sensors was placed inside the ceramic channels. The coil was weighed prior to each test. After a test, the wire was cleaned in acetone using an ultrasonic cleaner, washed with acetone and deoinized water, dried, and reweighed. The corrosion current density (rate), i_{corr}, in units of A/cm^2, was evaluated from the equation

$$i_{corr} = \frac{\Delta M}{M_0 A t} zF \tag{8}$$

where t is the time of exposure (in seconds) to the high temperature solution, A is the average of the initial and final surface areas of the coil (in cm^2), ΔM is the mass loss (in grams), M_0 is the composition averaged atomic mass of the steel, z is the oxidation number, and F is Faraday's constant.

2.6. Scanning electron microscopy and energy dispersive spectrometer studies

Scanning electron microscopy (SEM) was conducted to determine the changes in surface morphology and thickness of the wires prior to and following the corrosion experiments. An SEM energy dispersive spectrometer (EDS) was used to determine the ratios between chromium, iron, and nickel in the surfaces of the fresh (un-corroded) and corroded samples. The ratios were quantified by setting an 8–10 channel window centered on the main channel for each element and subsequently calculating the ratios between the integrated surfaces.

3. Results and discussion

3.1. Noise levels of potential and coupling current

As shown in Fig. 3, the potential and coupling current, ($E_0(t)$ and $I_0(t)$) display drifts as well as fluctuations in their time records. Thus, linear regression functions were generated for the potential and current over pre-selected periods. Then, the drifts were eliminated by

$$\delta E(t) = E_0(t) - E_{\mathrm{reg}}(t) \tag{9}$$

and

$$\delta I(t) = I_0(t) - I_{\mathrm{reg}}(t) \tag{10}$$

where $E_{\mathrm{reg}}(t)$ and $I_{\mathrm{reg}}(t)$ are the linear regression functions generated from $E_0(t)$ and $I_0(t)$, respectively, and $\delta E(t)$ and $\delta I(t)$ are the potential and current without drift (Fig. 4). The standard deviations for both potential and current, σ_{E} and σ_{I}, were then

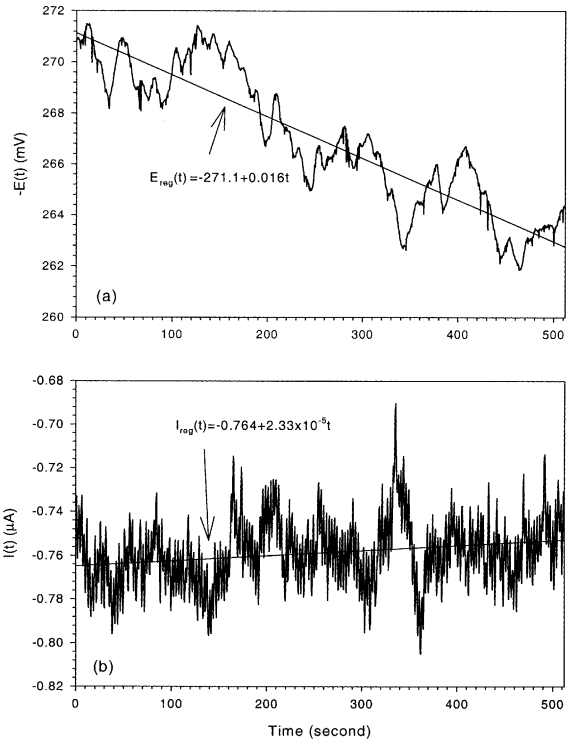

Fig. 3. Original records of potential (a) and coupling current (b) acquired from an EN sensor at a temperature of 350°C, pressure of 25 MPa, and flow rate of 0.5 ml/min in hydrogenated, 0.01 mol kg^{-1} HCl + 0.1 mol kg^{-1} NaCl.

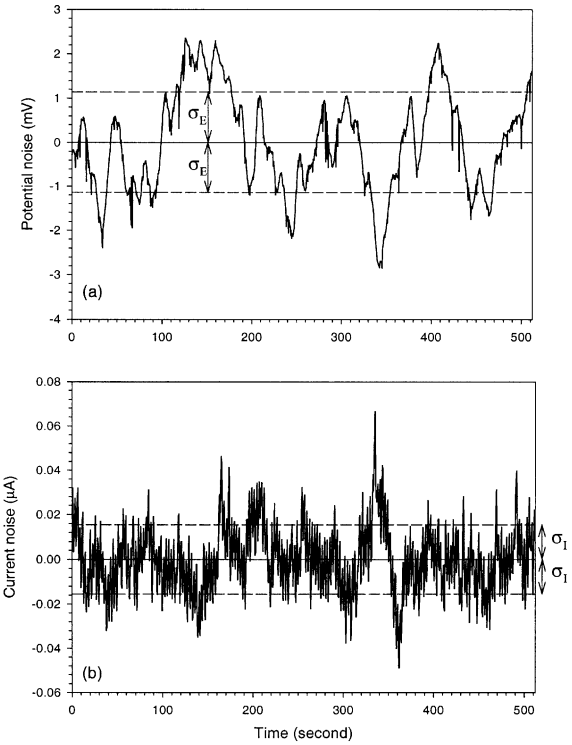

Fig. 4. Potential (a) and coupling current (b) records after removing drifts and DC components.

calculated from $\delta E(t)$ and $\delta I(t)$ using statistical software. Finally, the noise resistance (R_n) was calculated using Eq. (1).

3.2. Corrosion of Type 304 SS in subcritical and supercritical aqueous solutions

The surfaces of the Type 304 SS steel wires tested at 150°C were still bright after the tests. SEM examination of the surface (Fig. 5a) revealed that at 150°C, localized corrosion occurred, but that the corrosion features are not characteristic of typical pitting corrosion nor of active dissolution. After a one-week long test, no significant reduction in wire diameter was observed (Table 1). EDS results (Table 1) show that Fe was depleted and Cr was enriched on the surface or near sub-surface, presumably because of selective dissolution. At higher temperatures, Type 304 SS suffered from general corrosion (Fig. 5b) that resulted in a considerable reduction in wire diameter (Table 1). The ratio of Cr to Fe was less than that for 150°C.

By quantitatively analyzing Fe–Cr alloys using ESCA, Olefjord and Brox [26] found that the extent of enrichment of Cr and depletion of Fe on the surface and in the near sub-surface were functions of potential. The maximum enrichment of Cr was found at a potential in the region close to the active–passive transition. There

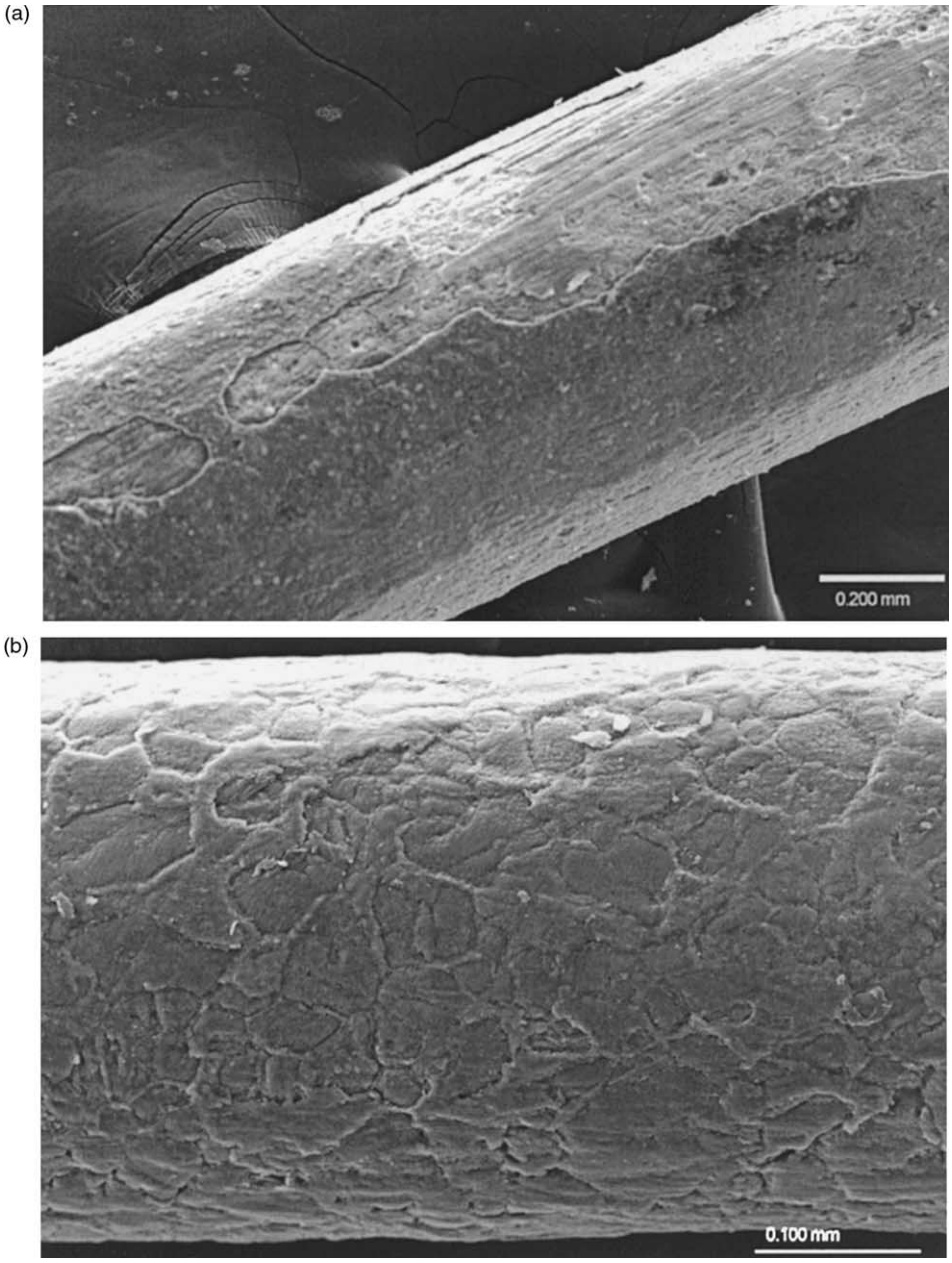

Fig. 5. SEM micrographs: (a) sample tested at 150°C for 168 h; (b) sample tested at 390°C for 1 h.

was some enrichment of Cr in the active region, but the enrichment was much less than that in the passive region. Thus, for 150°C, the corrosion state seems to be

Table 1
Summary of the results of SEM and EDS studies

	Average wire diameter (μm)	Cr:Fe	Cr:Ni	Fe:Ni
Uncorroded	490 ± 5	0.46:1	4.7:1	10.0:1
150°C (1 week)	480 ± 5	15.5:1	48.7:1	3.1:1
390°C (1 h)	350 ± 5	8.6:1	19.9:1	2.3:1

The diameter was measured directly under SEM. The ratio of elements was obtained from EDS analysis.

between active dissolution and complete passivity. At higher temperatures, Type 304 SS is in the active dissolution state.

The corrosion rate, which was found to be a function of temperature and flow rate (Fig. 6), is observed to pass through a maximum at about 350°C. Other investigators [16,27] have reported that the corrosion rate passes through a maximum at a near-critical temperature. The origin of the maximum in the corrosion rate has been previously explained using a phenomenological model that postulates competing effects of increasing temperature on the reaction rate constant and on the properties of the corrosive medium [27]. Thus, increasing temperature causes the reaction rate constant to increase via an Arrhenius relationship, but simultaneously results in a reduction in the dielectric constant of the medium, a decrease in the density of the solution and hence a reduction in volume-based concentrations, and in enhanced ion association, particularly as the system transitions from the subcritical to supercritical state. This model [27] predicts that the corrosion rate will pass through a maximum at a high subcritical temperature (330–370°C), depending upon the exact conditions, which is in good agreement with the present observations.

3.3. Corrosion rate and electrochemical noise resistance

As shown in Fig. 7a and b, under subcritical conditions, the corrosion rate of Type 304 SS is a linear function of flow rate, whereas, under supercritical conditions

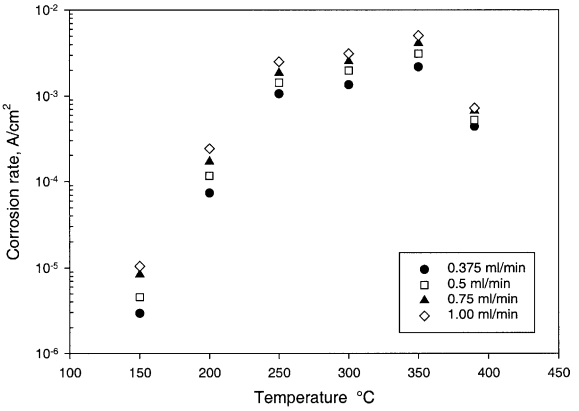

Fig. 6. Corrosion rate (current) evaluated using mass loss tests plotted as a function of temperature.

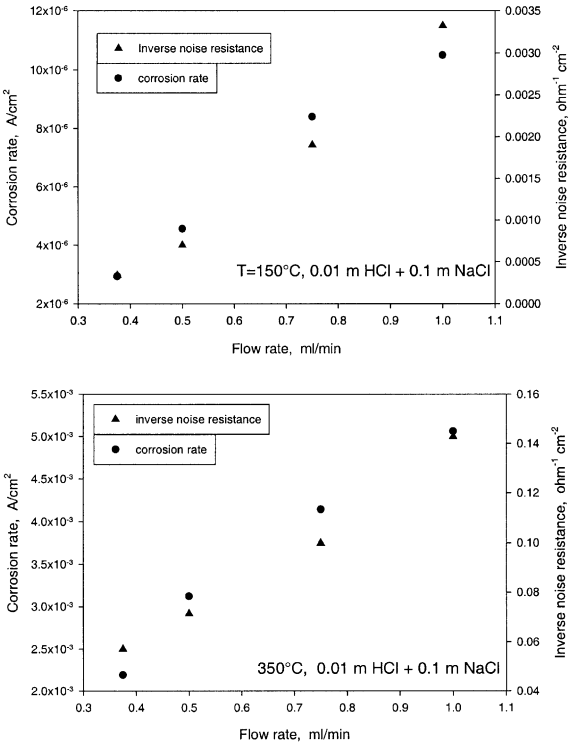

Fig. 7. Inverse noise resistance and corrosion rate as functions of flow rate for subcritical conditions.

(Fig. 8) at the highest flow rate, the dependence of corrosion rate on flow rate is found to deviate from this relationship. However, in both cases, the inverse noise resistance was in good correlation with the measured average corrosion rate.

Because the test solution was saturated with hydrogen, the cathodic reaction should be hydrogen evolution (due to the absence of oxygen) via the reduction of H^+

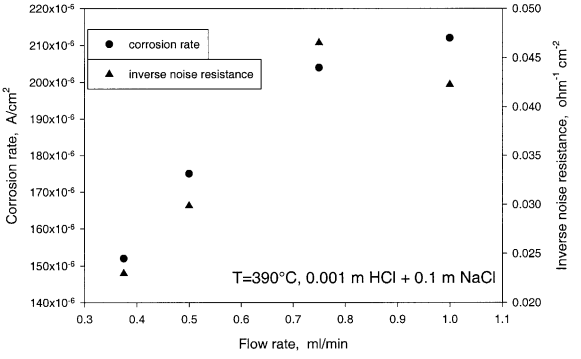

Fig. 8. Inverse noise resistance and corrosion rate as functions of flow rate for supercritical conditions.

or H_2O, or both. If so, then much, if not all, of the noise might be attributed to the detachment of hydrogen bubbles from the surface, as has been suggested by others for ambient temperature systems [5]. Thus, at high flow rates, hydrogen bubbles are expected to be more readily detached from the surface and hence the cathodic reaction and the whole corrosion process are presumably accelerated.

The relationship between the corrosion rate and the inverse noise resistance is exhibited in Fig. 9, in which the data are plotted on dual logarithmic scales. The results reveal that the corrosion rate is proportional to the inverse noise resistance at temperatures higher than 200°C.

3.4. Stern–Geary relationship

Stern and Geary [28] proposed that if the corrosion potential and current is determined by the intersection of the anodic and cathodic Tafel-type polarization curves, the Stern–Geary relationship (Eq. (2)) is valid and the Stern–Geary constant is given by

$$B = \frac{b_a b_c}{2.303(b_a + b_c)} \tag{11}$$

where b_a and b_c are, respectively, the Tafel parameters for the anodic and cathodic reactions. However, Stern's work [28–31] also shows that Eq. (11) is not always valid for other situations. In a review, Gabrielli and Keddam [32] considered five different corrosion scenarios: (1) the anodic and cathodic reactions are one step processes and are Tafelian electron transfer controlled; (2) the anodic reaction is a one step process and Tafelian electron transfer controlled, but the cathodic reaction is purely diffusion controlled; (3) the anodic reaction is a one step process and Tafelian electron transfer controlled, but the cathodic reaction is partly charge transfer and partly

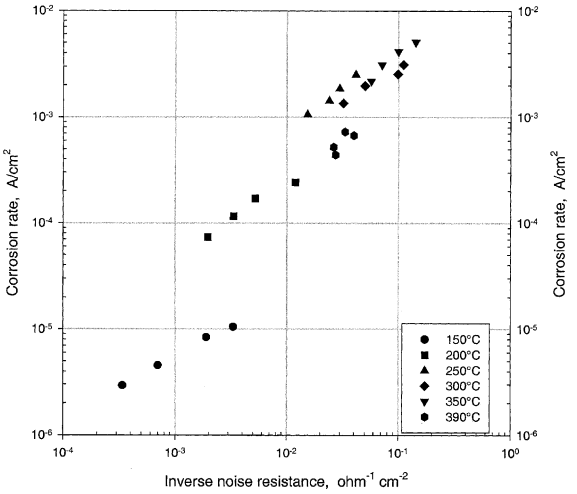

Fig. 9. Relation between corrosion rate and inverse noise resistance.

diffusion controlled; (4) both anodic and cathodic reactions are irreversible multiple step Tafelian processes, and; (5) the electrode is in the passive state. The authors concluded that only for the first mechanism, could the Stern–Geary constant be expressed by Eq. (11).

Actually, the relation between the corrosion rate and the inverse polarization resistance or the inverse noise resistance can be derived by considering the Butler–Volmer expression [33]. Thus, for the anodic reaction (dissolution of metal) the following applies:

$$i_a = \frac{e^{(2.303(E-E_{0,a}))/b_a}}{(1/i_{0,a}) + (1/i_{l,a})e^{(2.303(E-E_{0,a}))/b_a}} \tag{12}$$

and for the cathodic reaction (hydrogen evolution):

$$i_c = \frac{e^{(-2.303(E-E_{0,c}))/b_c}}{(1/i_{0,c}) - (1/i_{l,c})e^{(-2.303(E-E_{0,c}))/b_c}} \tag{13}$$

where $i_{0,a}$ and $i_{0,c}$ are, respectively, the exchange current densities for the anodic and cathodic reactions. $E_{0,a}$ and $E_{0,c}$ are, respectively, the equilibrium potentials of the anodic and cathodic reactions, E is the electrode potential, and $i_{l,a}$ and $i_{l,c}$ are, respectively, the limiting anodic and cathodic current densities. Since, at realistic corrosion potentials, normally, $i_{l,a} \gg i_{0,a}$, Eq. (12) can be simplified as

$$i_a = i_{0,a}e^{(2.303(E-E_{0,a}))/b_a} \tag{14}$$

which is a Tafelian type equation.

The total external current density (i) is an algebraic sum of the anodic and cathodic current and hence

$$i = \theta_a i_a - \theta_c i_c \tag{15}$$

where θ_a and θ_c are respectively surface coverage, of the anodic and cathodic regions, which may be functions of potential, pH, and flow rate.

For free corrosion conditions ($i = 0$), we have

$$i = 0 = \theta_a i_{0,a}e^{(2.303(E_{corr}-E_{0,a}))/b_a} - \theta_c \frac{e^{(-2.303(E_{corr}-E_{0,c}))/b_c}}{(1/i_{0,c}) - (1/i_{l,c})e^{(-2.303(E_{corr}-E_{0,c}))/b_c}} \tag{16}$$

where E_{corr} is the corrosion potential. Thus, from this above relation, we can derive the corrosion current (i_{corr}) by

$$i_{corr} = \theta_a i_{0,a}e^{(2.303(E_{corr}-E_{0,a}))/b_a} = \theta_c \frac{e^{(-2.303(E_{corr}-E_{0,c}))/b_c}}{(1/i_{0,c}) - (1/i_{l,c})e^{(-2.303(E_{corr}-E_{0,c}))/b_c}} \tag{17}$$

The definition of the linear polarization resistance is

$$\frac{1}{R_p} = \left[\frac{\Delta i}{\Delta E}\right]_{E=E_{corr}} \tag{18}$$

Taking into account Eqs. (15), (17), and (18), R_p can be expressed as

$$\frac{1}{R_p} = i_{corr}\left[\frac{1}{\theta_a}\left[\frac{\partial\theta_a}{\partial E}\right]_{E=E_{corr}} - \frac{1}{\theta_c}\left[\frac{\partial\theta_c}{\partial E}\right]_{E=E_{corr}}\right] + i_{corr}\frac{2.303(b_a+b_c)}{b_a b_c} - i_{corr}^2 \times \frac{2.303}{b_c i_{l,c}} \tag{19}$$

As can be seen from Eq. (19), the inverse polarization resistance $(1/R_p)$ or inverse noise resistance $(1/R_n)$ is not proportional to the corrosion current and the relationship between $1/R_p$ and i_{corr} depends on potential, pH, and flow rate, especially when θ_a and θ_c are not constants with respect to potential. However, when the first term on the right side of Eq. (19) is negligible, there are a number of cases where the inverse polarization resistance is proportional to the corrosion current. Below, three of the possible cases are considered:

(1) If the cathodic reaction is charge transfer controlled, i.e. $i_{l,c} \gg i_{corr}$, then

$$\frac{1}{R_p} = i_{corr}\frac{2.303(b_a+b_c)}{b_a b_c} \tag{20}$$

which is exactly the Stern–Geary relationship.

(2) If, however, the cathodic reaction is purely mass transport controlled, i.e. $i_{corr} = i_{l,c}$, then

$$\frac{1}{R_p} = i_{corr}\frac{2.303}{b_a} \tag{21}$$

(3) If the entire surface of the electrode is in the passive state and the anodic current is a constant with respect to potential, Eq. (19) is converted into:

$$\frac{1}{R_p} = i_{corr}\frac{2.303}{b_c} \tag{22}$$

For the above three cases, the ratio of the corrosion rate to the inverse noise resistance is a constant with respect to potential and flow rate.

Macdonald et al. [34] and Biswas [35] studied the polarization characteristics of hydrogen evolution/oxidation in basic solutions at elevated temperatures. Their experimental results showed that the cathodic limiting current was greater than 10^{-2} A/cm^2. Comparison between the limiting cathodic current and corrosion current evaluated via mass loss tests carried out in the present study suggests that the cathodic reaction under free corrosion conditions is not mass transport controlled. Because, at temperatures higher than 200°C, the corrosion state was not passive, but instead is one of active dissolution, Eq. (20), rather than Eqs. (21) and (22), should be the appropriate relationship between R_p and i_{corr}.

Fig. 9 clearly shows the proportionality between the corrosion rate and inverse noise resistance at temperatures higher than 200°C, whereas at 150°C the relation between the corrosion rate and inverse noise resistance significantly deviates from this relationship (i.e., slope in log–log space is less than 45°). The proportionality will not exist when the coverage of the anodic areas is a function of potential and flow rate, as shown by Eq. (19). However, there may be other reasons for the deviation of the proportionality at 150°C.

3.5. Sources of errors

Major complications are experienced with all polarization resistance measurements [36–43] as recently summarized by Scully [44]. They are: (1) anodic reaction of some other electroactive species (e.g. H_2 and Fe^{2+}), besides the corroding metal under investigation; (2) a change in the corrosion potential; (3) non-linear I–E dependence due to large ΔE; and (4) ohmic solution resistance. Other minor sources of errors were also examined [36,37], including the uses of an inaccurate oxidation number, z, average atomic mass, M_0, and Tafel parameters in determining the corrosion rate.

Indig and Groot [36,37] measured the corrosion rate of stainless steels and nickel-based alloys in lithiated water (basic) at 288°C via the linear polarization method and compared the results with the data generated using mass loss method. They found that the corrosion potentials of these alloys were within 50 mV of the equillibrium hydrogen electrode potential, and that the rate of dissolution of metals evaluated using the mass loss method was one-tenth of the total anodic current. Based on these observations, they concluded that the major source of error was that the hydrogen oxidation reaction, rather than the assumed dissolution of the metal, was the dominant anodic reaction.

One of the major differences between the present experiments and those of Indig and Groot was that the present experiments were conducted in corrosive acidic and chloride-containing aqueous solutions, while Indig and Groot's tests were conducted in non-corrosive aqueous solutions (i.e., in which the rate of the anodic partial reaction is small). We found that the corrosion rate at temperatures above 200°C was greater than 10^{-4} A/cm^2 (Fig. 9) while in Indig and Groot's experiment, the corrosion rate was about 10^{-6} A/cm^2 and the hydrogen oxidation rate was about 10^{-5} A/cm^2. Thus, in the case of the acidic solution, the dissolution of the metal, rather than the oxidation of hydrogen, was the dominant partial anodic reaction. We also found that, although the corrosion potential of Type 304 SS shifted in the noble direction and became closer to the equilibrium potential of the hydrogen electrode as the temperature increased, the potential difference between the Type 304 SS electrode and equilibrium hydrogen electrode ranged from -350 to -250 mV, while Indig and Groot observed in their tests that the potential difference between the SS electrodes and equilibrium hydrogen electrode was only 35–50 mV. Accordingly, the rate of hydrogen oxidation on the Type 304 SS electrodes in our experiments at temperatures above 200°C should be negligible with respect to the corrosion rate.

During the acquisition of the EN data, the ECP changed by about 10 mV (Fig. 3) and ΔE (the amplitude in the potential fluctuations) was about 2 mV (Fig. 4). Thus, the errors due to any change in the ECP during the measurements and due to the magnitude of ΔE are negligible. The conductance data for NaCl and HCl solutions have been summarized in one of our previous publication [45]. The calculated conductivity for 390°C was 1.87 S/cm. Noting that the cross-section of the path between the two EN electrodes was 0.5 mm by 10 mm, the resistance of the channel was found to be 1.6 Ω. The current flowing between the two electrodes shown in

Table 2
Stern–Geary constant, B^* ($I_{corr} = B^*/R_n$), evaluated via ENA and B $\{B = b_a b_c\ (b_a + b_c)\}$ evaluated via polarization measurements

Temperature (°C)	B^* (ENA) (V)	b_c (V)	b_a (V)	B (polarization) (V)
150	0.007	0.07	0.17	0.022
200	0.02	0.17	0.19	0.039
250	0.07	0.60	0.21	0.068
300	0.04	0.40	0.23	0.063
350	0.045	No data	No data	No data
390	0.008	No data	No data	No data

Fig. 3 is 0.78 μA. This gives a solution IR drop of 1.25×10^{-3} mV. Thus, the IR drop is negligible.

For the case of Type 304 SS, z could have any value between 2 and 3, depending on the oxidation state of each component metal, while M_0 could have a value between 51.996 and 58.71, depending on the composition of the steel. Thus, the errors due to inaccuracy of z and M_0 are relatively insignificant.

Because, the Tafel parameters appear in both numerator and denominator of Eq. (11), the evaluation based on Stern–Geary's equation is insensitive to changes of the Tafel parameters. However, large uncertainty in Tafel parameters could result in significant error in corrosion rate evaluation.

Tafel constants for both metal dissolution and hydrogen evolution at elevated temperatures up to 300°C were determined by Huang et al. [46], Macdonald et al. [34] and Biswas [35] using polarization measurements. We used the data in Refs. [34,35,46] to compare the ENA and mass loss methods. The Stern–Geary constants evaluated using the Tafel constants taken from Refs. [34,35,46] and employing Eq. (11), are presented in Table 2, together with values generated from the EN data. The discrepancy between the Stern–Geary constants evaluated by these two methods is 68% at 150°C, as a maximum, but is 3% at 250°C, as the minimum. No comparison was made at 350°C and 390°C, because no data for the Tafel constants are available. It is not surprising that there was significant error in the corrosion rate evaluated using ENA at 150°C. Firstly, the dependence of the corrosion rate on the inverse noise resistance was not linear. For this case, an equation other than Stern–Geary's equation should be used. Secondly, the corrosion rate at 150°C was from 10^{-6} to 10^{-5} A/cm^2. In this case, the corrosion rate might be comparable to the rate of hydrogen oxidation. Accordingly, the corrosion rate cannot be evaluated using the ENA method without knowing the rate of hydrogen oxidation.

4. Summary

The following conclusions can be drawn based on the study:

1. EN sensors have been developed for measuring corrosion rate in subcritical and supercritical aqueous systems, and the sensors have been evaluated in a contamination-free, flow-through electrochemical cell.

2. Mass loss tests were performed, and it was found that the corrosion rate of Type 304 SS is a function of temperature and flow rate. The corrosion rate of Type 304 SS was found to pass through a maximum at about 350°C, in agreement with theory.
3. The Stern–Geary relationship is a reasonable approximation for temperatures higher than 200°C. The corrosion rate can be quantitatively assessed from the inverse noise resistance using a Stern–Geary constant calculated from the Tafel constants for the anodic and cathodic reactions. However, the relationship between the corrosion rate and the inverse EN resistance deviates from proportionality at 150°C.
4. It is postulated that the deviation from the Stern–Geary relationship observed at 150°C is caused principally by the rate of hydrogen oxidation being comparable with the dissolution rate of the steel and because the steel was between the passive and active corrosion states.

Acknowledgements

The authors gratefully acknowledge the support of this work by the US Department of Energy (Grant DE-F607-96ER62303).

References

[1] T. Hagyard, J.R. Williams, Trans. Faraday Soc. 57 (1961) 2288.
[2] W.P. Inverson, J. Electrochem. Soc. 115 (1968) 617.
[3] K. Hladkey, J. Dawson, Corros. Sci. 22 (1981) 317.
[4] K. Hladkey, J. Dawson, Corros. Sci. 23 (1982) 231.
[5] J. Dawson, Electrochemical noise measurement: the definitive in situ technique for corrosion applications, ASTM STP 1277 (1966) 3.
[6] D.A. Eden, M. Hoffman, B.S. Skerry, Polymeric Materials for Corrosion Control, ACS Symposium Series, vol. 322, ACS, 1986, p. 36.
[7] C.-T. Chen, B.S. Skerry, Corrosion 47 (1991) 598.
[8] F. Mansfeld, H. Xiao, J. Electrochem. Soc. 140 (1993) 2205.
[9] H. Xiao, F. Mansfeld, J. Electrochem. Soc. 141 (1994) 2332.
[10] H. Xiao, L.T. Han, C.C. Lee, F. Mansfeld, Corrosion 53 (1997) 412.
[11] F. Mansfeld, C.C. Lee, J. Electrochem. Soc. 144 (1997) 2068.
[12] U. Bertocci, C. Gabrielli, F. Huet, M. Keddam, P. Rousseau, J. Electrochem. Soc. 144 (1997) 37.
[13] G. Gusmano, G. Montesperelli, S. Pacetti, A. D'Amico, Corrosion 53 (1997) 860.
[14] U. Bertocci, C. Gabrielli, F. Huet, M. Keddam, J. Electrochem. Soc. 144 (1997) 31.
[15] U. Bertocci, F. Huet, J. Electrochem. Soc. 144 (1997) 2786.
[16] C. Liu, D.D. Macdonald, E. Medina, J.J. Villa, J.M. Bueno, Corrosion 50 (1994) 687.
[17] D.D. Macdonald, C. Liu, M.P. Michael, Electrochemical noise measurements on carbon and stainless steel in high subcritical and supercritical aqueous environments, ASTM STP 1277 (1996) 247.
[18] M.P. Manahan Sr., D.D. Macdonald, A. Peterson, Corros. Sci. 37 (1995) 189.
[19] S. Liu, D.D. Macdonald, Fracture of AISI 4340 steel in concentrated sodium hydroxide solution, Corrosion Conference, NACE, paper no. 01236, 2001.
[20] A. Wensche, D.D. Macdonald, in press.
[21] S.N. Lvov, H. Gao, D.D. Macdonald, J. Electroanal. Chem. 443 (1998) 186.

[22] S.N. Lvov, H. Gao, D. Kouznetsov, I. Balachov, D.D. Macdonald, Fluid Phase Equilibria 150/151 (1998) 515.
[23] S.N. Lvov, X.Y. Zhou, D.D. Macdonald, J. Electroanal. Chem. 463 (1999) 146.
[24] S.N. Lvov, X.Y. Zhou, S.M. Ulyanov, A.V. Bandura, Chem. Geol. 167 (2000) 105.
[25] S.N. Lvov, X.Y. Zhou, S.M. Ulyanov, D.D. Macdonald, PowerPlant Chem. 2 (1) (2000) 5.
[26] I. Olefjord, B. Brox, Quantitative ESCA analysis of the passive state of an Fe–Cr alloy and an Fe–Cr–Mo alloy, Passivity of Metals and Semiconductors, Proceedings of the Fifth International Symposium on Passivity, Bombannes, France, Elsevier, 1983, p. 561.
[27] L.B. Kriksunov, D.D. Macdonald, J. Electrochem. Soc. 142 (1995) 4069.
[28] M. Stern, A.L. Geary, J. Electrochem. Soc. 104 (1957) 56.
[29] M. Stern, R.M. Roth, J. Electrochem. Soc. 104 (1957) 390.
[30] M. Stern, J. Electrochem. Soc. 104 (1957) 559.
[31] M. Stern, J. Electrochem. Soc. 104 (1957) 645.
[32] C. Gabrielli, M. Keddam, Corrosion 48 (1992) 794.
[33] A. Molander, G. Karlberg, Hydrogen water chemistry surveilance in boiling water reactor, Proceedings of the 4th International Symposium on Environmental Degradation of Materials in Nuclear Power Systems—Water Reactors (Houston, TX: NACE, 1990), pp. 4-156–4-163.
[34] D.D. Macdonald, S.N. Lvov, G. Kelkar, J.F. Magalhaes, H.-S. Kwon, A. Wuensche, R. Biswas, Z. Ahmed, G. Engelhardt, The development of deterministic methods for predicting corrosion damage in water cooled nuclear reactors, ESEERCO Report EP93-33, 1996.
[35] R. Biswas, Investigation of electrochemical phenomena in high temperature aqueous systems, Ph.D. Thesis, Pennsylvania State University, 1999.
[36] M.E. Indig, C. Groot, Corrosion 25 (1969) 455.
[37] M.E. Indig, C. Groot, Corrosion 26 (1970) 171.
[38] K.B. Oldham, F. Mansfeld, Corros. Sci. 13 (1973) 813.
[39] F. Mansfeld, J. Electrochem. Soc. 120 (1973) 515.
[40] F. Mansfeld, M. Kendig, Corrosion 37 (9) (1981) 556.
[41] R. Bandy, D.A. Jones, Corrosion 32 (1976) 126.
[42] M.J. Danielson, Corrosion 36 (4) (1980) 174.
[43] L.M. Callow, J.A. Richardson, J.L. Dawson, Brit. Corros. J. 11 (1976) 132.
[44] J.R. Scully, Corrosion 56 (2) (2000) 199.
[45] X.Y. Zhou, A. Bandura, S.M. Ulyanov, S.N. Lvov, Calculation of diffusion potentials in aqueous solutions containing HCl, NaOH and NaCl at temperatures from 25–400°C, Steam, Water and Hydrothermal Systems, Proceedings of the 13th International Conference on the Properties of Water and Steam, NRC CNRC, NRC Research Press, Ottawa 200, p. 480.
[46] S. Huang, K. Daehling, T.E. Carleson, M. Abdel-Latif, P. Taylor, C. Wei, A. Propp, Electrochemical measurements of corrosion of iron alloys in supercritical water, Supercritical Fluid Science and Technology, ACS, 1988, p. 287.